*J. Fluid Mech.* (2009), *vol.* 630, *pp.* 71–91.  
doi:10.1017/S0022112009006454 Printed in the United Kingdom

# A numerical investigation of horizontal viscous gravity currents

YANNICK HALLEZ[1,2] AND JACQUES MAGNAUDET[1,2]†

[1]Université de Toulouse; INPT, UPS; Institut de Mécanique des Fluides de Toulouse, Allée Camille Soula, F-31400 Toulouse, France

[2]CNRS, Institut de Mécanique des Fluides de Toulouse; F-31400 Toulouse, France

(Received 4 December 2008 and in revised form 4 February 2009)

We study numerically the viscous phase of horizontal gravity currents of immiscible fluids in the lock-exchange configuration. A numerical technique capable of dealing with stiff density gradients is used, allowing us to mimic high-Schmidt-number situations similar to those encountered in most laboratory experiments. Plane two-dimensional computations with no-slip boundary conditions are run so as to compare numerical predictions with the 'short reservoir' solution of Huppert (*J. Fluid Mech.*, vol. 121, 1982, pp. 43–58), which predicts the front position $l_f$ to evolve as $t^{1/5}$, and the 'long reservoir' solution of Gratton & Minotti (*J. Fluid Mech.*, vol. 210, 1990, pp. 155–182) which predicts a diffusive evolution of the distance travelled by the front $x_f \sim t^{1/2}$. In line with dimensional arguments, computations indicate that the self-similar power law governing the front position is selected by the flow Reynolds number and the initial volume of the released heavy fluid. We derive and validate a criterion predicting which type of viscous regime immediately succeeds the slumping phase. The computations also reveal that, under certain conditions, two different viscous regimes may appear successively during the life of a given current. Effects of sidewalls are examined through three-dimensional computations and are found to affect the transition time between the slumping phase and the viscous regime. In the various situations we consider, we make use of a force balance to estimate the transition time at which the viscous regime sets in and show that the corresponding prediction compares well with the computational results.

## 1. Introduction

Gravity currents are generated when a dense fluid (of density $\rho_2$) is released in a lighter one (of density $\rho_1$) or vice versa. Such flows are widely encountered in environmental and geophysical situations (storm outflows, avalanches and the like) (Hoult 1972; Simpson 1982) as well as in engineering problems (e.g. warm water discharges in cold water, spreading of fire gases and ventilation; Linden 1999). While theoretical models and extensive laboratory experiments have been devoted to this class of flows for a long time (see Simpson 1997 for an excellent review of the field up to the last decade), use of direct numerical simulation (DNS) to investigate them in detail is relatively recent. Most of the computational studies to date have focused on the early slumping phase of inertia-dominated currents during which the front velocity is roughly constant (e.g. Härtel, Meiburg & Necker 2000; Necker *et al.* 2005;

† Email address for correspondence: jacques.magnaudet@imft.fr

Cantero *et al.* 2007). This is of course partly because DNS can contribute to clarify several important open questions related to the internal structure of the flow during this phase. In contrast, the case of currents dominated by viscous effects or that of the late viscous phase of gravity currents initially dominated by inertia has not yet been widely addressed in DNS. As will become clear later, the main reason for this is that most of the numerical techniques used in previous investigations do not allow this viscous phase to be properly computed. In the present paper we employ DNS to focus on the transition from the slumping phase to the subsequent viscous regime(s) and on the characteristics of these viscous regimes themselves in the case of an instantaneous fixed-volume release in the lock-exchange configuration.

More precisely, we consider a semi-infinite horizontal channel of height $H$ closed by a vertical wall located at $x = -L_0$ and containing a volume $V_0 = L_0 H$ (in the two-dimensional case) of dense fluid restrained by a lock placed at $x = 0$. This lock is instantaneously opened at $t = 0$ so that a gravity current develops, the front position of which is located at $x_f(t)$. We assume molecular diffusion and surface tension effects to be negligible, so that the two fluids only mix owing to hydrodynamic effects, and no capillary regime has to be considered. In the whole paper, we only consider small density differences compatible with the Boussinesq approximation. All the computational results to be discussed are issued from two-dimensional simulations in plane channels except those of § 2 and § 3.3 in which intrinsically three-dimensional configurations are considered. In what follows we normalize lengths and time by $H$ and $\sqrt{H/g'}$, respectively ($g' = g(\rho_2 - \rho_1)/\rho_2$ denoting the reduced gravity) and mark the resulting dimensionless quantities with a tilde. To clarify the *raison d'être* of some of the issues addressed in this paper, a brief discussion of the various successive regimes that can be expected in the above configuration is in order.

If viscosity is neglected, the solution at early times is that of the dam-break flow problem, namely

$$\tilde{x}_f = Fr\,\tilde{t}, \tag{1.1}$$

where $Fr = (\mathrm{d}x_f/\mathrm{d}t)/\sqrt{g'H}$ is the Froude number. In a well-known paper (Benjamin 1968) it was shown that $Fr = 0.5$ for an energy-conserving current. However, high-Reynolds-number experiments rather indicate $0.45 < Fr < 0.5$ (see e.g. Marino, Thomas & Linden 2005), a difference due to small wall-friction effects (Bonometti, Balachandar & Magnaudet 2008). Equation (1.1) characterizes the slumping phase. If the receding front reaches the endwall during this phase, then $\tilde{x}_f = \tilde{L}_0$ for $\tilde{t} = \tilde{T}_S$ such that

$$\tilde{T}_S = \tilde{L}_0 Fr^{-1}. \tag{1.2}$$

For much larger times ($\tilde{x_f} \gg \tilde{L}_0$) and provided viscous effects are still negligible, a self-similar regime during which buoyancy is balanced by inertia is approached. This is the inertial phase during which the current length in a plane channel obeys (Huppert & Simpson 1980)

$$\tilde{l}_f = \tilde{x}_f + \tilde{L}_0 = 1.47\tilde{V}_0^{1/3}\tilde{t}^{2/3}. \tag{1.3}$$

In contrast, if inertia is negligible right after the opening of the gate or if it is long before the receding front reaches the endwall, the current is self-similar with (Gratton & Minotti 1990)

$$\tilde{x}_f = \alpha Re^{1/2}\tilde{t}^{1/2}, \tag{1.4}$$

where the flow Reynolds number is defined as $Re = g'^{1/2}H^{3/2}/\nu$ ($\nu$ denoting the kinematic viscosity) and $\alpha = 0.0922$ in the two-dimensional case (Hinch *et al.* 2007)

or $\alpha = 0.0739$ in a cylindrical horizontal tube (Séon *et al.* 2007), $H$ being the tube diameter in the latter case. This solution holds until the receding front reaches the endwall, say for $\tilde{t} = \tilde{T}_V$ such that

$$\tilde{T}_V = Re^{-1}(\tilde{L}_0/\alpha)^2. \tag{1.5}$$

Then the solution ceases to be self-similar.

On the other hand, if inertia is negligible and $\tilde{x_f} \gg \tilde{L}_0$, a different self-similar asymptotic corresponding to the point-source approximation is approached in which

$$\tilde{l}_f = \beta Re^{1/5}\tilde{V}_0^{3/5}\tilde{t}^{1/5} \tag{1.6}$$

in a two-dimensional channel (Huppert 1982) or

$$\tilde{l}_f = \beta_c Re^{1/4}\tilde{V}_0^{1/2}\tilde{t}^{1/4} \tag{1.7}$$

in a horizontal cylindrical tube (Takagi & Huppert 2007), the prefactors $\beta$ and $\beta_c$ being 1.133 and $(12/35)^{1/4} \approx 0.765$, respectively. For convenience, the viscous regimes with $\tilde{x}_f \sim \tilde{t}^{1/2}$ and $\tilde{l}_f \sim \tilde{t}^{1/5}$ or $\tilde{l}_f \sim \tilde{t}^{1/4}$ will be referred to as the long reservoir (LR) and short reservoir (SR) regimes, respectively.

Several of these predictions have been convincingly validated experimentally, while some others still deserve confirmation. Generally, experiments performed with axisymmetric currents (Didden & Maxworthy 1982; Huppert 1982) or with currents propagating in cylindrical tubes (Séon *et al.* 2007; Takagi & Huppert 2007) have been more conclusive because influence of the boundaries is better controlled. Many other configurations involving viscous gravity currents have been considered as well but will not be discussed here. A comprehensive review of the field was given by Huppert (2000).

In order to predict the succession of regimes experienced by a given current, the characteristic transition times to each regime have to be compared. In particular, for given flow conditions, it is first necessary to determine whether the inertial solution (1.3) or the SR viscous solution (1.6) occurs after the receding current hits the endwall. This can be determined by noting that the inertial phase is observed only if the dimensionless height of the resulting current goes below 0.075, which requires $\tilde{l}_f > \tilde{l}_{f\,I} = 13.33\tilde{V}_0$ according to the box-model prediction (Huppert & Simpson 1980). Moreover the transition length $\tilde{l}_{f\,SR}$ and time $\tilde{T}_{SR}$ at which the viscous force associated with the dam-break solution (1.1) starts to exceed that corresponding to the SR solution (1.6) after the current has been influenced by the endwall obey (Huppert & Simpson 1980)

$$\tilde{l}_{f\,SR} = Re^{2/7}\tilde{V}_0^{5/7}, \tag{1.8}$$

$$\tilde{T}_{SR} = Re^{3/7}\tilde{V}_0^{4/7}. \tag{1.9}$$

Hence the inertial phase can exist only if $\tilde{l}_{f\,I} < \tilde{l}_{f\,SR}$, which implies $Re \gtrsim 8650\tilde{V}_0$. Given the moderate Reynolds numbers used in the computations to be described below, this condition will never be met in this paper. Therefore the inertial regime (1.3) will be ignored in what follows, and we will only be concerned with situations in which the slumping phase solution (1.1) is followed either by the viscous LR solution (1.4) (which sets in for $\tilde{t} = \tilde{T}_{LR}$) or by the SR solution ((1.6) which sets in for $\tilde{t} = \tilde{T}_{SR}$ or (1.7)) or by both. More precisely, the succession of phases to be observed will depend on how $\tilde{T}_S$, $\tilde{T}_{SR}$, $\tilde{T}_V$ and $\tilde{T}_{LR}$ compare to each other.

Based on the above discussion, the structure of the present paper is as follows: Section 2 briefly describes the numerical techniques we use and shows that they allow a

faithful reproduction of the characteristics of viscous gravity currents involving nearly immiscible fluids. Section 3 describes computational results which, to our knowledge, provide the first clear validation of the theoretical predictions for the viscous LR and SR regimes in two-dimensional channels, i.e. (1.4) and (1.6), respectively. We then discuss the consequences of the effects of an $O(1)$ Schmidt number on previous computational predictions and examine the influence of sidewalls in experiments through three-dimensional computations and force-balance arguments. In § 4 we first make use of computational results to derive and validate a theoretical criterion predicting which type of viscous regime immediately succeeds the slumping phase. In the case in which the slumping phase is followed by the LR regime, we show that a secondary viscous transition from the LR regime to the SR regime later occurs and determine theoretically the corresponding transition time. Computations also help understand the gradual evolution of the current from the time the receding front hits the endwall to that at which the resulting disturbance reaches the front of the advancing current. In particular, they reveal that, under certain conditions, the LR regime can even set in a short time after the receding front has hit the endwall. We finally summarize our main conclusions in § 5 and present a unified diagram of the various evolutions a given viscous current may follow.

## 2. Numerical approach and validation

Most DNS of gravity currents reported in the literature made use of spectral or pseudo-spectral techniques because they offer excellent accuracy even with a moderate number of grid points (see Härtel *et al.* 2000; Necker *et al.* 2002, 2005; Cantero *et al.* 2007). However the numerical stability of these methods is compromised when sharp gradients have to be dealt with, such as the density gradient across the front of a high-Schmidt-number gravity current. (The Schmidt number is defined as the ratio of the kinematic viscosity to the binary molecular diffusion coefficient.) The usual remedy has been to stabilize the corresponding computations by considering a diffusion term in the density equation. Therefore the predictions made in the aforementionned studies correspond to a Schmidt number of order unity. This has almost no influence on the predictions during the slumping phase in which inertia effects dominate and is indeed representative of realistic conditions for viscous gazeous gravity currents. However most laboratory experiments make use of liquids (essentially fresh and salt water) for which the Schmidt number is rather $O(10^3)$. To our knowledge, the only attempt to compute the viscous phase of a gravity current using a spectral approach has been that of Cantero *et al.* (2007) in which the viscous-spreading law was found to be closer to the $l_f \sim t^{3/8}$ prediction of Hoult (1972) for a gravity current flowing on a fluid surface than to the expected result of Huppert (1982). One can of course suspect the difference to be due to Schmidt number effects, as the theoretical model assumes that the released volume is strictly conserved and that the interface between the two fluids is kept sharp, which, at late times, is only true if molecular diffusion has negligible effects. In particular, a recent study by Bonometti & Balachandar (2008) points out that the front thickens tremendously with time in low-Reynolds-number gravity currents with an $O(1)$ Schmidt number.

Based on these remarks, it is clear that a different numerical strategy is required to obtain reliable computational predictions of high-Schmidt-number viscous gravity currents which can be compared with theoretical predictions and most laboratory experiments. Obviously, the key point is to select a technique capable of handling stiff density profiles. To this end, we use the in-house JADIM code. This code was originally

developed to compute two-phase incompressible flows of immiscible fluids with highly contrasted densities, especially bubbly flows (e.g. Bonometti & Magnaudet 2006, 2007). Here surface tension is set to zero, since we do not wish to consider the capillary regime of gravity currents. In the above finite-volume code, the transport equation for the local volume fraction of the heavy fluid (which is identical to that of the density field) is solved using a flux-corrected scheme. More precisely, the transport equation is split into successive one-dimensional sub-steps, one along each grid direction. Within each sub-step, the corresponding advective flux is discretized using a Zalesak scheme (Zalesak 1979) which combines the use of a low-order (here first-order) and a high-order (here fourth-order) spatial discretization to preserve positivity and monotonicity of the volume fraction and to ensure second-order spatial accuracy. The momentum equations, in which no reference to the Boussinesq approximation is made, are discretized using second-order centred schemes. Time advancement is achieved through a Runge–Kutta (RK3)/Crank–Nicholson algorithm. The incompressibility condition is finally satisfied at the end of each time step, using a variable-density projection technique. Overall, the code is second-order accurate in space and first-order accurate in time, owing to the Euler scheme employed to advance the density equation.

It has to be pointed out that while the set of equations used here corresponds to immiscible fluids, since molecular diffusivity is set to zero, the treatment of the density field on a discrete grid prevents the interface between the two fluids from remaining infinitely sharp. Actually, the density is found to vary from $\rho_1$ to $\rho_2$ over one to three grid cells, resulting in a large but finite effective Schmidt number. Bonometti & Balachandar (2008) employed the same code and showed the effective numerical Schmidt number to be $O(10^3)$, which is typical of experiments performed with liquids. This is essentially a qualitative estimate, since the numerical Schmidt number at a given point of the flow depends on the local grid size and orientation of the front with respect to the grid. Therefore a proper choice of the grid size has to be made to ensure that the front thickness remains much less than the viscous diffusion scale everywhere. Moreover, since this numerical diffusion spreads the interface over one to three cells, it would be impossible to obtain an accurate description of immiscible gravity currents at very late stages, when the current height is less than a few cells. We took care of these various aspects to ensure that the simulations presented in the paper are sufficiently resolved at all times. We refer the reader to Hallez & Magnaudet (2008) for more details on the numerical technique as well as for validations with gravity-driven flows confined in tilted tubes and to Bonometti *et al.* (2008) for results obtained with the same code in non-Boussinesq density currents.

The computations to be described below were run in the lock-exchange configuration defined in § 1, either in two-dimensional or three-dimensional channels or in cylindrical tubes. The length-to-height (or length-to-diameter) ratio ranges from 32 to 102. The corresponding grids involve 80 nodes in the vertical direction for two-dimensional channels and $48^2$ nodes in the cross-section for three-dimensional channels. In the streamwise direction, the number of grid points ranges from 512 to 3168 for all geometries, depending on the length-to-height ratio. The density ratio is set to $\rho_2/\rho_1 = 1.008$. We assume the dynamic viscosity to be the same in both fluids, which implies that the kinematic viscosity is slightly larger in the light fluid.

Prior to discussing new findings provided by these computations, we find it useful to describe a validation test corresponding to a well-documented case, namely that of a current propagating in a long cylindrical tube with the lock located midway between the two endwalls, i.e. starting from an initial symmetric configuration. This

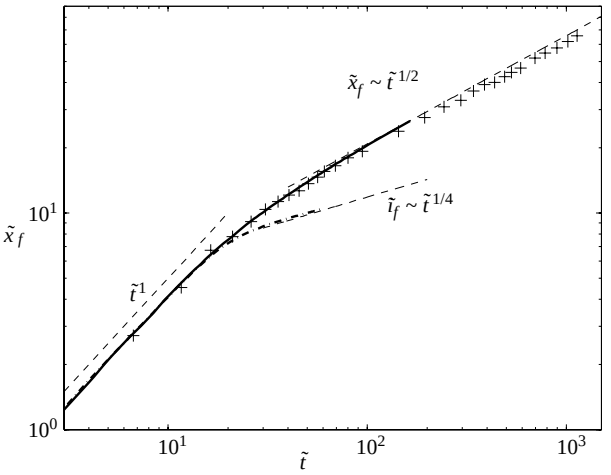


FIGURE 1. Evolution of the front position in a current resulting from a release in a cylindrical tube: $-\cdot-\cdot-$, computational result for a short release ($\tilde{L}_0 = 1$); ——: computational result for a symmetric release (here $\tilde{L}_0 = 17$); $+++$, experimental data from Séon *et al.* (2007); the thin dashed lines indicating the $t^{1/2}$ and $t^{1/4}$ regimes were plotted using the theoretical prefactors $\alpha = 0.0739$ and $\beta_c = (12/35)^{1/4}$ determined by Séon *et al.* (2007) and Takagi & Huppert (2007), respectively.

problem was addressed, both theoretically and experimentally, by Séon *et al.* (2007). We computed the same physical situation using the experimental set of parameters. The tube was discretized with 32 nodes in the radial direction and 64 nodes in the azimuthal direction. The evolution of the front position recorded in the experiment performed under conditions $Re = 790$ and $\rho_2/\rho_1 = 1.008$ with almost immiscible liquids (fresh and salt water) is plotted in figure 1, together with the corresponding computational prediction.

The theoretical prediction (1.4) obtained by the same authors for the LR regime is also reported for comparison. Computational results display an excellent agreement with experimental data all along the flow evolution which includes a slumping phase, a transitional stage and an LR viscous phase. Another computational result corresponding to a short release ($\tilde{L}_0 = 1$) is added with the corresponding theoretical prediction (1.7). In the latter case, the agreement on the time exponent is again excellent, and the numerical prefactor in (1.7) is recovered within 1 %.

From the above comparison, we conclude that our numerical technique accurately reproduces the experimental and theoretical results of both Séon *et al.* (2007) and Takagi & Huppert (2007) for the LR and SR viscous regimes in a horizontal cylindrical tube, respectively. Therefore we are confident that our code will allow us to carry out numerical experiments to explore various aspects of viscous gravity currents of immiscible fluids.

## 3. Predictions and experiments in plane channels

### 3.1. *Predictions in the LR regime*

In two dimensions, the theoretical prediction for the LR regime (1.4) (with $\alpha = 0.0922$) has not yet received any experimental validation. Figure 2($a$) reports the results of several computations we ran to check this prediction, using large heavy fluid releases with $\tilde{L}_0 > 17$ to ensure that the current becomes viscously dominated before it

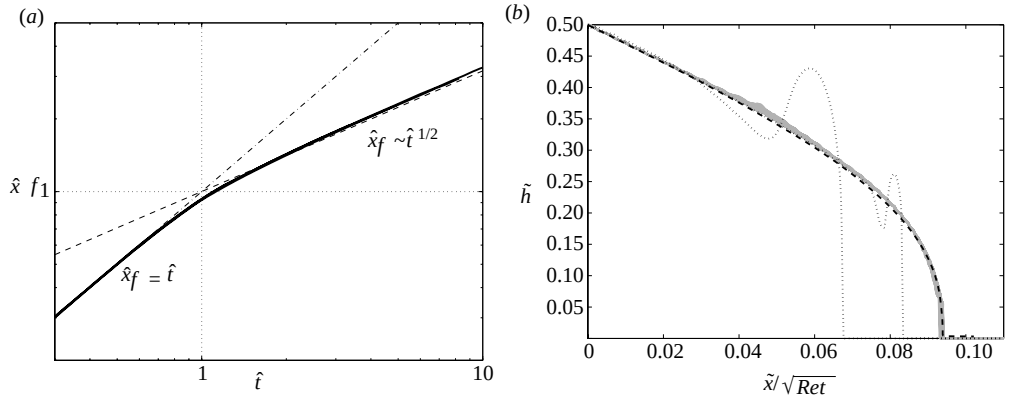


FIGURE 2. (*a*) Evolution of the front position in a two-dimensional current reaching the LR viscous regime: computational results for $Re = 200,\ 400,\ 600$ and 790 (black lines) all collapse on the master curve defined by $\hat{x}_f = \hat{t}$ for $\hat{t} < 1$ and $\hat{x}_f = \hat{t}^{1/2}$ for $\hat{t} > 1$; (*b*) theoretical and computational predictions for the current profile corresponding to $Re = 200$; – – –, theoretical prediction (3.3); ——, computational results taken at 45 successive times during the viscous phase; · · · ·, two profiles obtained during the development of the viscous phase.

reaches the nearest endwall. In this figure, the front position $\tilde{x}_f$ and time $\tilde{t}$ have been rescaled by the transition position $\tilde{x}_{f\,LR}$ and time $\tilde{T}_{LR}$ to the LR regime at the considered Reynolds number so that we define $\hat{x}_f = \tilde{x}_f/\tilde{x}_{f\,LR}$ and $\hat{t} = \tilde{t}/\tilde{T}_{LR}$. The transition takes place at the time at which the viscous force associated with the slumping solution starts to exceed that associated with the LR viscous solution. Equivalently, the transitional characteristics can be computed by equating the front positions predicted by (1.1) and (1.4), which yields

$$\tilde{x}_{f\,LR} = \alpha^2 ReFr^{-1}, \tag{3.1}$$

$$\tilde{T}_{LR} = \alpha^2 ReFr^{-2}. \tag{3.2}$$

Introducing $\hat{x}_f$ and $\hat{t}$, (1.1) and (1.4) reduce to $\hat{x}_f = \hat{t}$ and $\hat{x}_f = \hat{t}^{1/2}$ respectively, whereas the transition obviously takes place at $(\hat{x}_{f\,LR}, \hat{t}_{LR}) = (1, 1)$. With this renormalization, all computational curves collapse on a single master curve valid all along the current life. The difference between the time exponent (respectively the numerical prefactor) predicted by (1.4) and that found in computations is less than 1 % (respectively 2 %) for sufficiently well-established self-similar states. Hinch *et al.* (2007) also showed the current height to be governed by

$$\frac{\partial \tilde{h}}{\partial \tilde{t}} = \frac{1}{3} Re \frac{\partial}{\partial \tilde{x}} \left[ \tilde{h}^3 (1 - \tilde{h}^3) \frac{\partial \tilde{h}}{\partial \tilde{x}} \right]. \tag{3.3}$$

The normalized current profile recorded at 45 successive times during the LR regime of a current corresponding to $Re = 200$ is plotted in figure 2(*b*). This profile is found to follow closely the theoretical prediction obtained by integrating (3.3). The two profiles corresponding to early stages of the flow indicate that the self-similar viscous profile is settled progressively, starting from the initial lock position. At early times, the local inertia/gravity balance results in a sharp profile with a prominent blob, and this picture holds until viscous effects dominate the front dynamics.

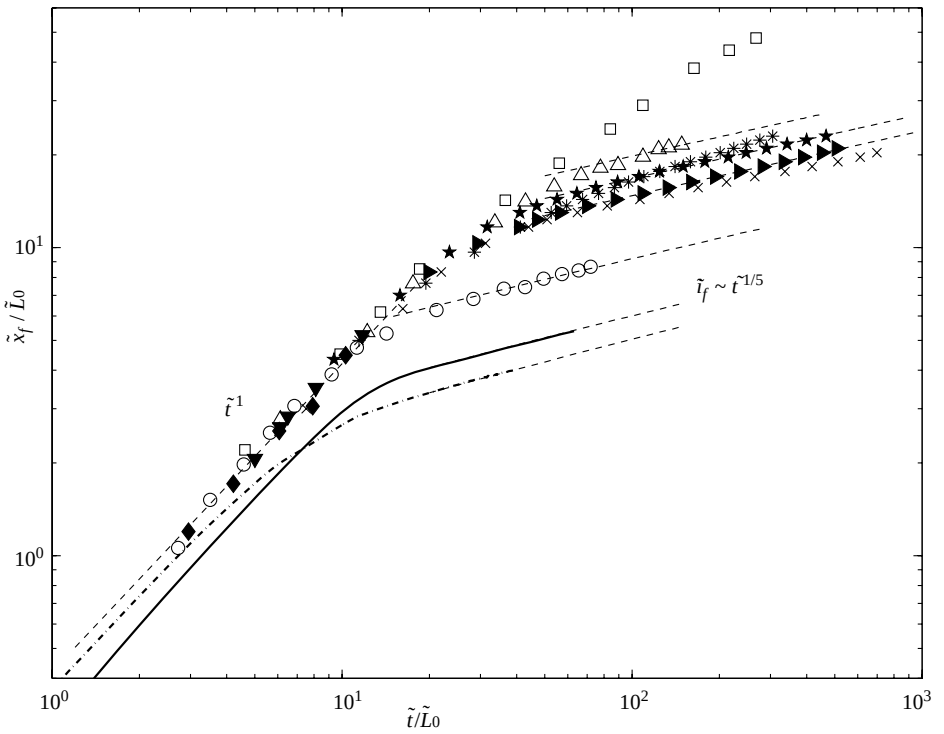


FIGURE 3. Distance travelled by the front for various releases leading to the SR regime ($\tilde{h_0} = 1$ except specified otherwise). Experiments of Rottman & Simpson (1983): ○, $l_{fSR}/L_0 = 6$; ◆, $l_{fSR}/L_0 = 10$; △, $l_{fSR}/L_0 = 12$; ▼, $l_{fSR}/L_0 = 18$; □, $l_{fSR}/L_0 = 25$. Present experiments: ►, $l_{fSR}/L_0 = 9.5$; *, $l_{fSR}/L_0 = 10.8$, $\tilde{h_0} = 1/6$; ×, $l_{fSR}/L_0 = 10.7$; ★, $l_{fSR}/L_0 = 10.8$; +, $l_{fSR}/L_0 = 10.8$, $\tilde{h_0} = 1/6$. Computational results: ——, $x_{fSR}/L_0 = 3.04$, $Re = 200$; –·–·–, $x_{fSR}/L_0 = 2.5$, $Re = 790$; – – –, $\tilde{l}_f \sim \tilde{t}^{1/5}$.

### 3.2. *Predictions and experiments in the SR regime*

The prediction (1.6) derived by Huppert (1982) for the SR viscous regime has been checked in several experiments, especially those of Rottman & Simpson (1983). Nevertheless, the slopes inferred from the corresponding data reveal a significant variability. More precisely, the slopes deduced from figure 12 of the latter paper lead to time exponents between 0.23 and 0.27 approximately, which suggests a 1/4 exponent rather than the 1/5 exponent predicted by (1.6). A similar variability may be observed in the results of Marino *et al.* (2005) and is nicely illustrated in figure 9(*d*) of the paper by Cantero *et al.* (2007). (Note that there is a small misprint in this figure, the time exponent displayed by the solid line being actually −4/5). We also carried out some additional experiments in an horizontal 4 m long channel, 0.25 m wide and 0.5 m high. The two fluids were clear water and dyed salt water. In order to reach the SR regime, we performed lock exchanges with small volumes of salt water of typical density 1050 kg m$^{-3}$. The initial lengths $L_0$ of the released volumes were 0.044 m, 0.095 m or 0.15 m, and their initial heights $h_0$ were about 0.06 m, whereas different total heights $H$ of fresh water were employed. The evolution of $\tilde{x}_f$ in the experiments of Rottman & Simpson (1983) and in our own experiments is reported in figure 3. The various runs correspond to different values of $l_{f\,SR}/L_0$ (see (1.8) for the definition of $l_{f\,SR}$). The time exponent deduced from our experiments ranges from

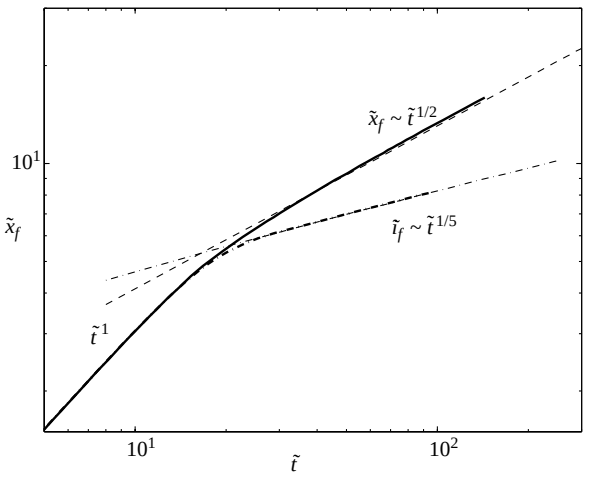


FIGURE 4. Distance travelled by the front of a two-dimensional current as a function of time for $Re = 200$: ——, LR regime reached with $\tilde{L}_0 = 17$); –·–·–, SR regime reached with $\tilde{L}_0 = 1.5$. The thin dashed (respectively dot-dashed) line corresponds to the prediction (1.4) (respectively (1.6) with a prefactor set to $0.93\beta$).

0.15 to 0.27, these extreme two values being obtained with the same set of parameters (namely $\rho_2/\rho_1$, $Re$, $\tilde{L}_0$ and $\tilde{h}_0$). Finally, the evolution of the two currents of figure 3 that exhibit a 1/5 time exponent corresponds to an 'experimental' prefactor in (1.6) higher than its theoretical counterpart $\beta$ by 18 % and 22 %, respectively. There may be multiple reasons for the large variability observed among experimental results. In particular, small perturbations generated by the opening of the gate may affect the free surface (an effect which does not exist in cylindrical tubes), and there may be small local variations in the slope of the channel. Also, even though the channels used in experiments have large aspect ratios, the flow is actually three-dimensional, owing to the no-slip condition imposed by the lateral walls. We will come back to this point later.

We ran several computations in the above situation with different Reynolds numbers and initial volumes. The corresponding results are displayed in figures 3 and 4. In particular, figure 4 shows the computed evolution of the front position for $Re = 200$ and two contrasted released volumes: a very short volume $\tilde{L}_0 = 1.5$ and a much longer one $\tilde{L}_0 = 17$. The run with $\tilde{L}_0 = 17$ corresponds to the LR solution and is only reported here for comparison. In contrast, the run with $\tilde{L}_0 = 1.5$ confirms that, after the slumping phase, a current generated by a sufficiently small release evolves in agreement with the SR self-similar solution (1.6). The numerical time exponent and prefactor are found to be $0.198 \pm 0.001$ and $0.93\beta$, respectively. More generally, all computations leading to an SR viscous regime predict the 1/5 exponent with less than 2 % difference, despite the finite length of the domain. The prefactor is always found to lie between $0.86\beta$ and $1.02\beta$. The above comparison indicates that present computations recover the theoretical self-similar prediction characterizing the SR viscous phase.

Cantero *et al.* (2007) also briefly considered this regime but found the exponent of the front position to be closer to that corresponding to a gravity current flowing over another fluid (Hoult 1972), i.e. $\tilde{l}_f \sim \tilde{t}^{3/8}$, and the computational prefactor was more than $3\beta$. We strongly suspect the discrepancy to be due to the $O(1)$ Schmidt number

used in these pseudo-spectral computations to ensure numerical stability. Indeed, such a large molecular diffusivity significantly reduces density gradients, which results in two effects. In the horizontal direction, the driving force is reduced, which in turn reduces the velocity of the current, at least for short times (Bonometti & Balachandar 2008). In the vertical direction, the current thickens dramatically, which reduces the velocity gradient at the bottom wall and thus the resistive viscous force. In particular, the characteristic length in the viscous stress is not the current height $h(x)$ anymore but rather the penetration thickness $\sqrt{\nu t}$. Equating the gravitational driving force with the viscous force then leads to the scaling $\tilde{l}_f \sim \tilde{t}^{3/8}$ found by Hoult (1972) instead of the $\tilde{t}^{1/5}$ scaling, in line with the observations of Cantero *et al.* (2007). Note that even though theoretical solutions for viscous currents with $Sc = O(1)$ are not available, it is obvious that the self-similar behaviour (1.6) cannot subsist under such circumstances. This is made clear by considering the equation governing the reduced density $(\rho(\tilde{z}) - \rho_1)/(\rho_2 - \rho_1)$ whose integral across the current height yields the governing equation for $\tilde{h}(\tilde{x}, \tilde{t})$. When molecular diffusion is absent, this equation is of the Reynolds type, leading to the self-similar solution (1.6). In contrast, when finite diffusion effects are present, it involves an additional diffusion flux at the interface, which leads to a modified evolution of $\tilde{h}$. Based on this remark, it is clear that SR viscous currents computed with spectral methods making use of an $O(1)$ Schmidt number cannot obey the scaling (1.6).

Beyond such $O(1)$ Schmidt numbers dictated by numerical constraints, an $O(1)$ effective Schmidt number may also be encountered in the front region and along the interface in turbulent currents with immiscible fluids. In this context, one can also question the validity of (1.6) once such currents become viscously dominated, since turbulent diffusion may well have spread the interface between the two fluids in a way pretty similar to molecular diffusion. This could lead to results close to those obtained by considering laminar currents with an $O(1)$ Schmidt number. If this happens to be the case, and we assume that finite-Schmidt-number effects result in a gradual shift in the time exponent of the evolution law from 1/5 to 3/8, it could explain the variability observed among the experiments, since they were generally carried out under turbulent conditions over a broad range of Reynolds number. Three-dimensional high-Schmidt-number/high-Reynolds-number DNS could help check this conjecture.

### 3.3. *Three-dimensional effects*

To assess possible alterations of two-dimensional predictions by flow three-dimensionality, we ran several three-dimensional computations in a channel of aspect ratio unity with either periodic conditions or no-slip conditions in the spanwise direction. A small disturbance was added to the initial density profile to trigger the transition to three-dimensionality in the former case. When the released volume is large enough for the LR regime to occur, both types of three-dimensional currents exhibit a $t^{1/2}$ evolution in the LR regime (figure 5*a*). Streamwise vortices are well visible on the body of the currents (figures 6*a* and 7*a*). Neither their spanwise spacing nor their typical strength seems to be significantly altered by the nature of the boundary condition on the sidewalls. More significant differences can be detected on the shape of the current fronts: as may be seen in figure 6(*b*), the no-slip condition on the sidewalls generates a marked rim at the extremities of the front, while the central part is pretty flat. The front is found to be steeper in presence of periodic lateral conditions with a clear presence of lobe and cleft structures (figure 7*b*). In presence of periodic boundary conditions, the front velocity is almost the same as that of the two-dimensional current, even though a tiny decrease of the distance travelled by the

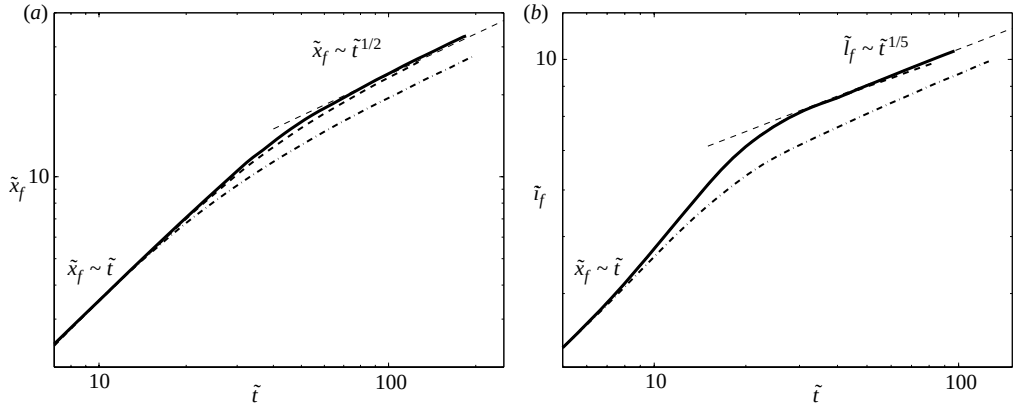


FIGURE 5. Comparison of the evolution of two- and three-dimensional currents at $Re = 200$ for a large release (LR) with $\tilde{L}_0 = 17$ ($a$) and a small release (SR) with $\tilde{L}_0 = 1.72$ ($b$) in a channel of aspect ratio $A = 1$: ——, two-dimensional current; – – –, three-dimensional current with periodic conditions in the spanwise direction; – · – · –, three-dimensional current with no-slip conditions on the sidewalls. The thin dashed line in figure 5($a$) (respectively $b$) corresponds to the prediction (1.4) (respectively (1.6) with a prefactor set to $0.914\beta$).

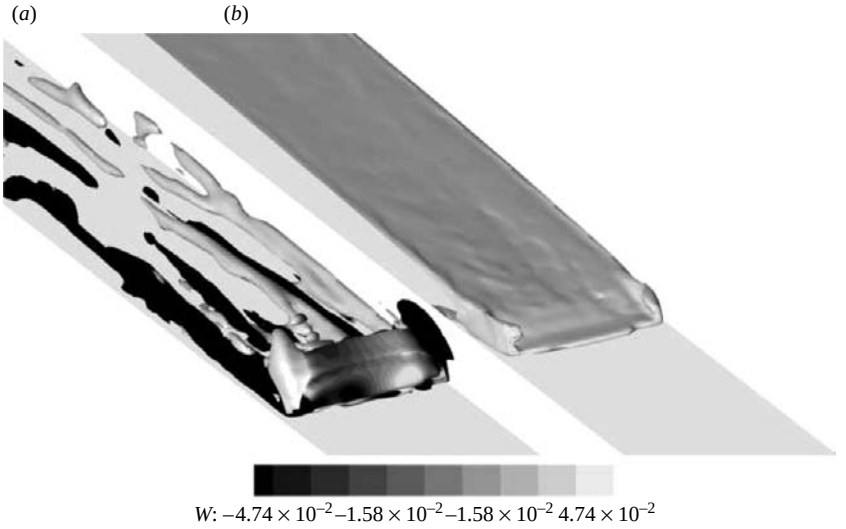


FIGURE 6. Structure of a three-dimensional current in the LR regime with no-slip boundary conditions in the spanwise direction ($Re = 660$). ($a$) Vortical structures coloured by the strength $W$ of the streamwise vorticity normalized by $\sqrt{g'/H}$; ($b$) current surface plotted using the $(\rho - \rho_1)/(\rho_2 - \rho_1) = 0.65$ isosurface. The spatial scales are identical on both axes.

front may be detected in figure 5($a$). This decrease certainly results from the small additional dissipation induced by the streamwise structures.

In contrast, compared to the two-dimensional reference, the transition from the slumping phase to the LR regime occurs significantly earlier for the current with no-slip conditions on the sidewalls. This is a direct consequence of the increased drag resulting from the presence of the lateral boundary layers. A rough estimate of the impact of this additional drag on the transition time to the LR regime may be achieved by evaluating the time $\tilde{T}_{LR*}$ at which the total viscous force starts to exceed

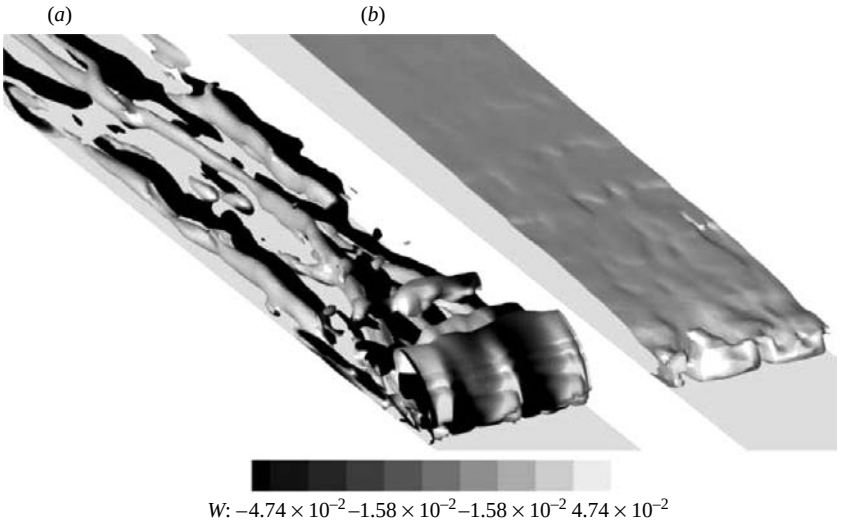


FIGURE 7. Same as in figure 6 with periodic boundary conditions in the spanwise direction.

the inertial force assuming that the dimensionless thickness of the lateral boundary layers is $\tilde{\delta}(\tilde{t})$, while the bottom boundary layer is fully developed at that time and has a constant dimensionless thickness $K/2$. Equating the transition time $\tilde{T}_{LR}$ given by (3.2) with that provided by this momentum balance in the two-dimensional case yields $K = (2\alpha/Fr)^2$. Then, in the three-dimensional case, the viscous force is increased by $1 + K/(2A\tilde{\delta}(\tilde{t}))$, where $A$ denotes the channel aspect ratio, i.e. the width-to-height ratio. Provided the lateral boundary layers are still developing when $\tilde{t} = \tilde{T}_{LR*}$, which is the case as long as $\tilde{T}_{LR*} < Re\ A^2/4$, one has $\tilde{\delta}(\tilde{T}_{LR*}) \approx Re^{-1/2}\tilde{T}_{LR*}^{1/2}$. Therefore the transition time now obeys

$$\tilde{T}_{LR*}(1 + K(Re/\tilde{T}_{LR*})^{1/2}/2A) \approx K\,Re/4. \tag{3.4}$$

Equation (3.4) predicts that in the case of figure 5($a$) (where $Re = 660$), the transition is advanced by about 43 % with respect to the two-dimensional situation. We determined the transition time graphically from this figure by intersecting the $t^1$ and $t^{1/2}$ lines tangent to the initial and final stages of the computational curves, respectively. This method provides $\tilde{T}_{LR*} = 27.1$, while the two-dimensional result is $\tilde{T}_{LR} = 46.3$, indicating that the transition is advanced by about 41.5 %, in good agreement with the above prediction. We also examined three-dimensional effects in currents resulting from much shorter releases leading to a direct transition from the slumping phase to the SR viscous regime. As shown in figure 5($b$), the corresponding currents exhibit a $t^{1/5}$ evolution, whatever the boundary condition in the spanwise direction. Possible three-dimensional effects in this regime were already considered by Didden & Maxworthy (1982) who studied currents with a constant inflow in channels of large aspect ratios. Using their estimates for all three forces in balance right at the time of the transition, it can be shown that the two-dimensional estimate (1.9) for this time is reduced by $(1 - 2Re^{-1}\tilde{t}/A\tilde{\delta}(\tilde{t}))^{3/7}$. Therefore, three-dimensional effects affect the corresponding transition time according to

$$\frac{\tilde{T}_{SR*}}{(1 - 2(\tilde{T}_{SR*}/Re)^{1/2}/A)^{3/7}} \approx Re^{3/7}\tilde{V}_0^{4/7}. \tag{3.5}$$

In the case of the computations presented in figure 5(*b*) (where $Re = 200$), (3.5) predicts that three-dimensional effects decrease the transition time by about 23 %. Again, we also determined the transition time graphically from this figure by intersecting the corresponding $t^1$ and $t^{1/5}$ lines. This technique yields $\tilde{T}_{SR*} = 14.2$, while the two-dimensional result is $\tilde{T}_{SR} = 19.0$. The difference corresponds to a 25 % decrease, in good agreement with the above prediction.

To conclude, the three-dimensionality of the flow does not alter the two-dimensional self-similar scaling found for either LR or SR currents. The only discernible effect in both regimes is the decrease of the transition time (or position) due to the enhanced friction exerted on the currents by the lateral walls. Therefore it turns out that the variability of the evolution law of the front observed in the various experiments is not due to the three-dimensionality of the flow.

## 4. Prediction of successive regimes in a given current

### 4.1. *Prediction of the earliest viscous regime*

The results presented in § 3 highlight the possibility to obtain either of the two scalings (1.4) and (1.6) in a given channel, depending on the released volume and flow Reynolds number. Therefore it is desirable to derive a criterion predicting whether the LR or SR viscous regime first succeeds the slumping phase. This goal may be achieved by comparing the transition times to the LR and SR viscous regimes, $\tilde{T}_{LR}$ and $\tilde{T}_{SR}$. Given the direct transition from the slumping phase to a viscous regime in present computations, the transition position and time for the LR regime are provided by (3.1) and (3.2), respectively. The change of slope at point (1, 1) in figure 2 confirms these predictions. On the other hand, processing the data of figure 3 indicates that predictions (1.8) and (1.9) are fairly well recovered, both in experiments and in computations, when the slumping phase is succeeded by the SR regime. Therefore (1.9) appears as a relevant estimate of $\tilde{T}_{SR}$. Then, expressing the condition $\tilde{T}_{LR} < \tilde{T}_{SR}$ provides the minimum released volume $\tilde{V}_{0\,c}$ required for the LR viscous regime to succeed the slumping phase. This condition is written as

$$\frac{\tilde{V}_{0\,c}}{Re} = \left(\frac{\alpha}{Fr}\right)^{7/2}, \tag{4.1}$$

where $\alpha = 0.0922$ is the numerical prefactor involved in (1.4). (Note that since only two-dimensional currents are considered in this section, $\tilde{V}_0$ may be replaced by $\tilde{L}_0$ everywhere it appears.) We validated this criterion using 17 runs performed at Reynolds numbers ranging from 200 to 790 with various initial lengths $\tilde{L}_0$ smaller or larger than $\tilde{L}_{0c}$. The result of this validation is displayed in figure 8. Only in a narrow band located along the critical curve is there some doubt on the nature of the viscous regime that sets in after the slumping phase. Interestingly, $Fr$ is known to increase with Reynolds number towards Benjamin's (1968) prediction, $Fr = 0.5$, and is roughly constant for $Re > O(10^3)$, a condition achieved in most real flows. As a consequence, the relation (4.1) becomes quasi-linear at high Reynolds number and simplifies to $\tilde{V}_{0\,c} = (3.3 \pm 0.6)10^{-3} Re$ for $0.45 < Fr < 0.5$. This condition can also be reversed to infer that given a released volume $\tilde{V}_0$ the Reynolds number must be lower than $O(300\tilde{V}_0)$ for the LR regime to occur.

### 4.2. *The possible secondary viscous transition*

As soon as the SR regime sets in, the current extends from one endwall to its head. Then the reservoir cannot be considered infinite any more, and the condition required

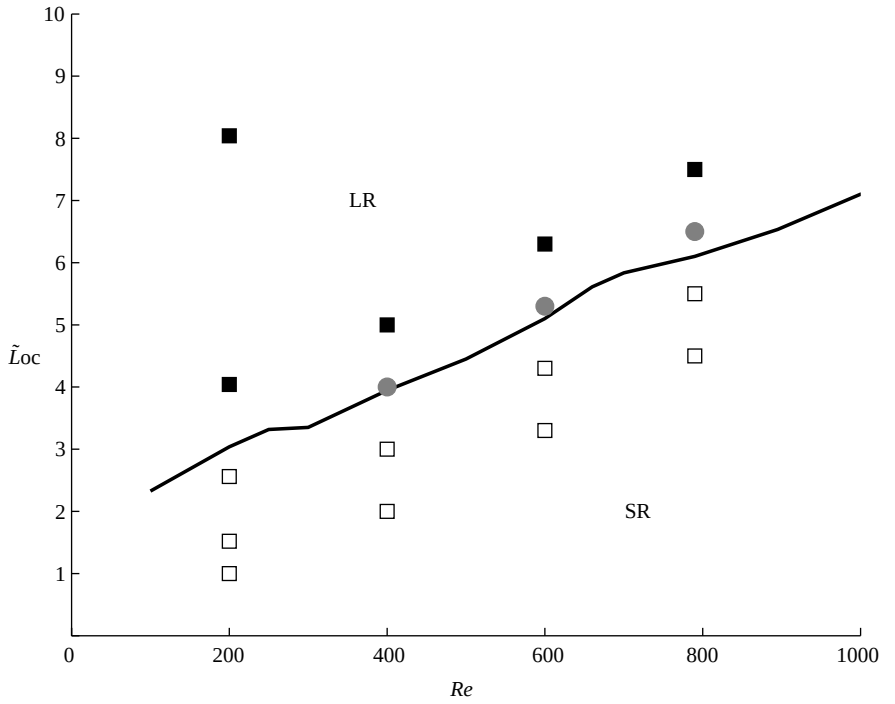


FIGURE 8. Critical length $\tilde{L}_{0c}$ of the released volume required for the LR regime to succeed the slumping phase. Solid line: relation (4.1) evaluated using the Froude number obtained numerically. Each symbol corresponds to a two-dimensional computational run: ■, the LR regime succeeds the slumping phase; □, the LR regime cannot occur and the slumping phase is directly succeeded by the SR regime; ●, intermediate cases for which the nature of the viscous regime that succeeds the slumping phase is difficult to determine unambiguously.

to reach the LR regime can never be fulfilled at later time; i.e. the current stays in the SR regime whatever $\tilde{t} > \tilde{T}_{SR}$. In contrast, if the slumping phase is succeeded by the LR regime, one can wonder whether the current can later experience a second transition from the LR regime to the SR regime. Referring to the characteristic times defined in the introduction, this could in principle be the case at late times if $\tilde{T}_{LR}$ is shorter than the time $\tilde{T}_S$ at which the receding current would hit the wall if it were staying in the slumping phase. Under this condition, the LR regime is expected to exist within a finite time interval, say $\tilde{T}_{LR} < \tilde{t} < \tilde{T}_V$, approximately, $\tilde{T}_V$ being the time at which the current hits the endwall during the LR regime. Then, for $\tilde{t} \gg \tilde{T}_V$, the conditions for the SR regime to occur are in principle fulfilled. To validate this scenario, we ran long computations with large enough released volumes. Figure 9 confirms that in such cases, the second viscous transition expected from the above argument indeed happens. More precisely, as predicted by (4.1), the current experiences a direct transition from the slumping phase towards the SR regime in cases in which $\tilde{L}_0 < \tilde{L}_{0c}$ (□ in figure 8, ◇ and ◁ in figure 9). When $\tilde{L}_0$ is close to $\tilde{L}_{0c}$, the current reaches the LR regime but immediately departs from it towards the SR regime (● in figure 8). Finally, for larger releases, the current first reaches the LR regime and remains in this regime for a while. However, after the receding front has hit the wall, the viscous current eventually switches to the SR regime (■ in figure 8, □ and ▽ in figure 9).

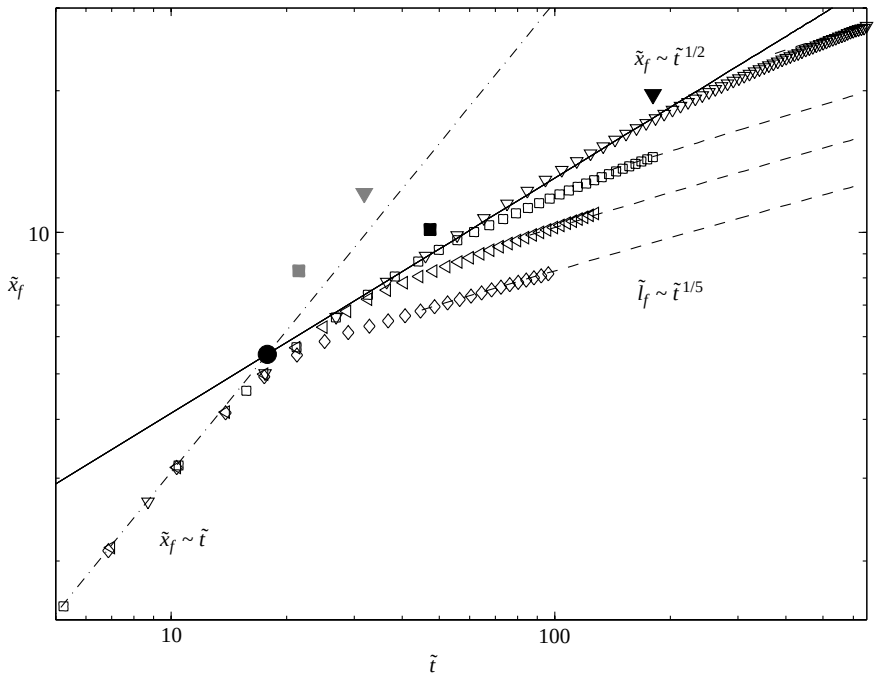


FIGURE 9. Evolution of the distance travelled by a two-dimensional numerical current corresponding to $Re = 200$ ($\tilde{L}_{0c} = 2.87$) for various released volumes: $\diamond$, $\tilde{L}_0 \simeq 1.52$; $\triangleleft$, $\tilde{L}_0 \simeq 2.56$; $\square$, $\tilde{L}_0 \simeq 4.04$; $\triangledown$, $\tilde{L}_0 \simeq 8.04$, $-\cdot-\cdot-$, slumping phase (1.1); ——, LR regime (1.4); – – –, SR regime (1.6); ●, transition from the slumping phase to the LR phase as predicted by (3.1) and (3.2); grey symbols: transition from the slumping phase to the SR regime as predicted by (1.8) and (1.9) for the largest two releases; black symbols: secondary viscous transition as predicted by (4.4) and (4.5) for the largest two releases. To compute these transitions, $\beta$ was set to 0.986 to be consistent with the computational prefactor obtained in the SR regime.

The physical mechanism at work in this second transition may be better understood from figure 10 which compares the evolution of the current shape during a 'pure' LR regime without any endwall effect (say current 1) with that of a current during the transitional phase from the LR to the SR regime (say current 2). As can be seen in figure 10(*b*)–(*e*), a disturbance propagates downward after the receding front of current 2 hit the wall, even though the current dynamics are already fully controlled by viscous effects. Nevertheless, the velocity of the front of current 2 does not change immediately (figure 10*b*, *c*). Rather, the fronts of both currents still follow the same evolution until the disturbance reaches the front of current 2 (figure 10*d*). At this point, the front of current 2 starts moving more slowly (figure 10*e*) and eventually joins the $\tilde{t}^{1/5}$ evolution. It is of interest to notice that the above mechanism is similar to that observed by Rottman & Simpson (1983), even though in their case the current dynamics were still dominated by inertia at the time the receding current hit the wall. In particular they noticed that the advancing current did not 'feel' the endwall immediately but rather started to be affected only when the bore generated by the interaction of the receding current with the endwall reached the front. In the present computations, when the current is still dominated by inertial effects at the time of the reflection, the disturbance also takes the form of a bore propagating at the surface of the heavy fluid. This is easily discernible on space–time diagrams of the current height (see figure 6 of Rottman & Simpson 1983 for instance). In contrast, when

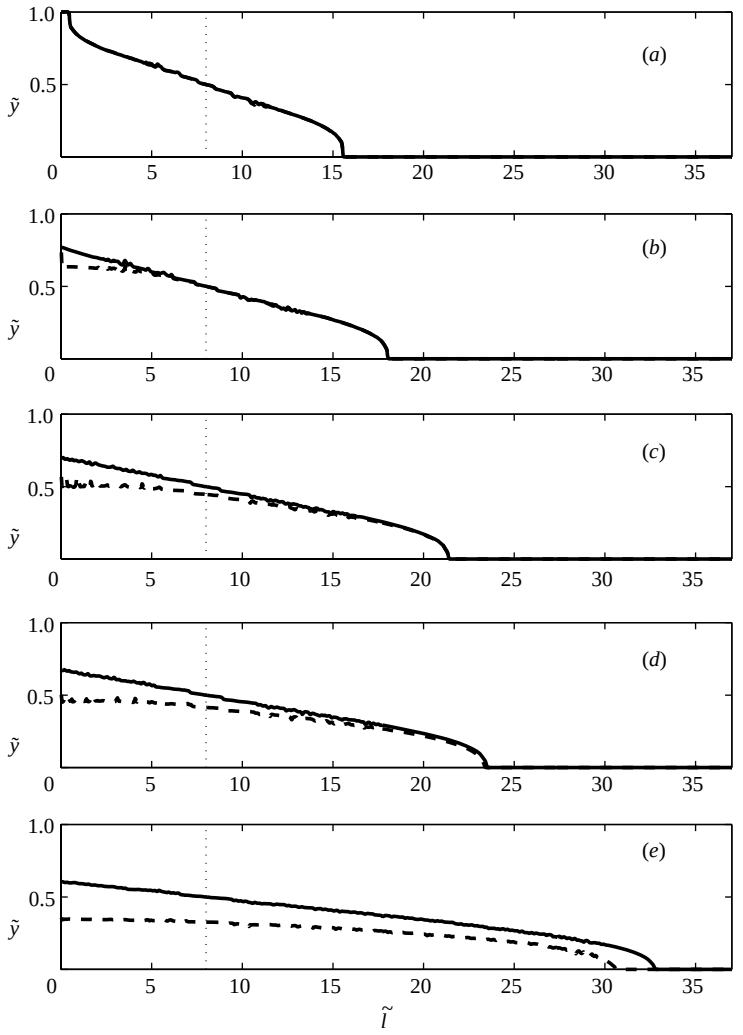


FIGURE 10. Evolution of the profile of two currents corresponding to $Re = 200$: ——, current 1 with $\tilde{L}_0 \gg 1$ (the left wall is rejected far outside the figure); – – –, current 2 with $\tilde{L}_0 = 8.04$ (the left wall corresponds to the left side of the figure). Current 1 is in the LR regime on all snapshots. (*a*) Current 2 is in the LR regime. (*b*) and (*c*) The receding current has reached the endwall; the profile of current 2 is altered behind the front of the disturbance while its head is still in the LR regime. (*d*) The disturbance just reaches the head of current 2. (*e*) Current 2 slows down and switches to the SR regime.

the current is already in the LR viscous phase at the time of the reflection, as in figure 10, the disturbance merely consists in a local modification of the shape of the current that can only be detected through a comparison with the profile of an undisturbed current. The position of the front of the disturbance is easily detected in figure 10(*b*, *c*), whereas it is hard to infer from figure 10(*d*,*e*) the exact time at which the flow regime of current 2 changes. A much better tool for this is provided by space–time diagrams of the local height difference between current 1 and current 2 such as that of figure 11 to be discussed later. Using such diagrams, we found that

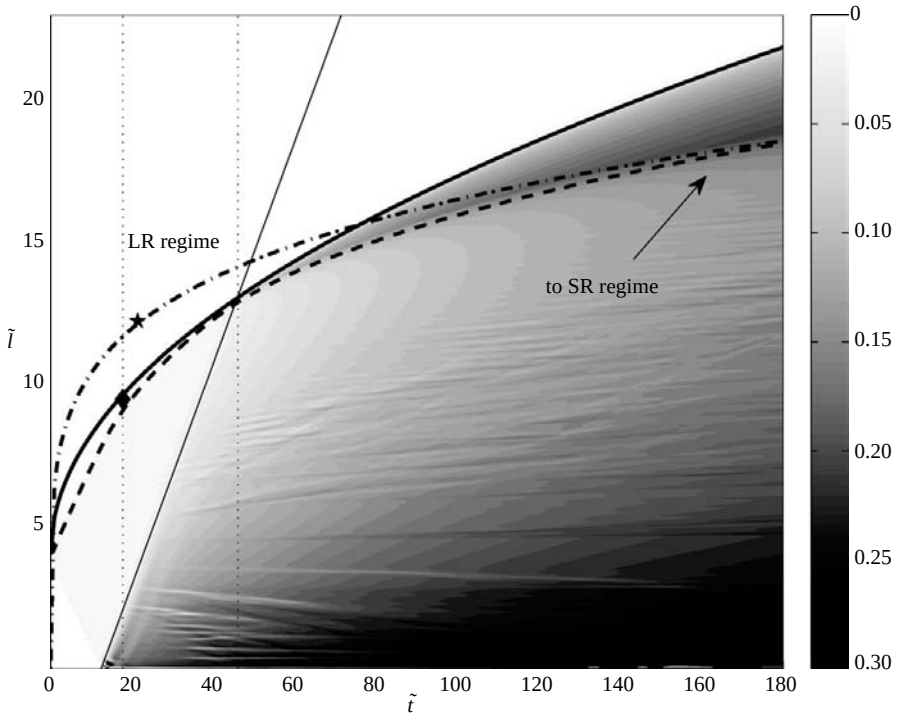


FIGURE 11. Space–time diagram showing the height difference $\Delta\tilde{h}(\tilde{x},\tilde{t})$ (in greyscale) between current 1 with $L_0 \gg 1$ and current 2 with $L_0 = 4.04$ (both currents correspond to $Re = 200$): – – –, position of the front of current 2; ——, LR solution (1.4) with $\alpha = 0.094$; – · – · –, SR solution (1.6) with $\beta = 0.974$; ◆, position of the transition from the slumping phase to the LR regime as predicted by (3.1) and (3.2); ★, position of the transition from the slumping phase to the SR regime as predicted by (1.8) and (1.9).

the regime of the current always changes right at the time at which the disturbance catches the front.

The secondary viscous transition is expected to take place at the time $\tilde{t} = \tilde{T}_{LS}$ at which the viscous force corresponding to the LR solution starts to exceed that corresponding to the SR solution. During the LR regime, the dimensionless force associated with the bottom viscous stress and the buoyancy force balance each other. The typical magnitude of the former force is $Re^{-1}\tilde{u}_f\tilde{x}_f/\tilde{h}_{LR}$, while that of the latter is $\tilde{h}_{LR}^2/2$, where $\tilde{h}_{LR}$ and $\tilde{u}_f$ denote the dimensionless averaged thickness and front velocity of the current, respectively. Using (1.4) and noting that $\tilde{u}_f = \mathrm{d}\tilde{x}_f/\mathrm{d}\tilde{t}$, this first balance implies

$$\tilde{h}_{LR} = \alpha^{2/3}. \tag{4.2}$$

Then, during the SR regime, the length $\tilde{l}_f$ of the current is given by (1.6). The above momentum balance then yields

$$\tilde{h}_{SR}(\tilde{t}) = \left(\frac{2}{5}\right)^{1/3} \beta^{2/3} \left(\frac{\tilde{V}_0^2}{Re}\right)^{1/5} \tilde{t}^{-1/5}. \tag{4.3}$$

The viscous forces in the two regimes must match at the transition time $\tilde{t} = \tilde{T}_{LS}$, so that the balance of (4.2) and (4.3) provides

$$\tilde{T}_{LS} = \left(\frac{2}{5}\right)^{5/3} \left(\frac{\beta}{\alpha}\right)^{10/3} \frac{\tilde{V}_0^2}{Re} \approx 930 \frac{\tilde{V}_0^2}{Re}. \tag{4.4}$$

Equation (1.6) implies in turn

$$\tilde{l}_{f\,LS} = \beta Re^{1/5} \tilde{V}_0^{3/5} \tilde{T_{LS}}^{1/5} \approx 4.44 \tilde{V}_0. \tag{4.5}$$

Interestingly, setting $\tilde{x}_f = -\tilde{L}_0$ in (1.4) indicates that the receding current hits the endwall at $\tilde{t} = \tilde{T}_V = (\tilde{L}_0/\alpha)^2/Re$. Hence the prediction (4.4) implies that $\tilde{T}_{LS}$ is about 7.9 times larger than $\tilde{T}_V$. Figure 9 qualitatively confirms the above prediction for $\tilde{T}_{LS}$, even though the transition time is difficult to locate precisely, owing to the progressive nature of the transition.

### 4.3. *Late occurrence of the LR regime*

An important ingredient in the derivation of (1.4) lies in the symmetry of the problem with respect to the lock position. This suggests that the LR regime can only be reached as long as the endwalls are far enough from the front of the advancing and receding currents. However our observations indicate that under certain conditions, a transitional LR evolution can arise even after the receding current has hit the endwall. Figure 11 illustrates the existence of such a late transition in the form of a space–time diagram representing the local height difference $\Delta\tilde{h}(\tilde{t}, \tilde{l})$ between current 1 with $\tilde{L}_0 \gg 1$ (for which endwalls have no influence) and current 2 with $\tilde{L}_0 = 4.04$ (which corresponds to the square symbols in figure 9). In the latter case, the receding front hits the endwall at $\tilde{t} = \tilde{T}_S \approx 12$, while the transition from the slumping phase to the LR regime is only expected to occur at $\tilde{t} = \tilde{T}_{LR} \approx 18$ according to (3.2). Indeed, for $0 \leqslant \tilde{t} \leqslant \tilde{T}_{LR}$, the front position of both currents is found to evolve linearly (see the dashed line in figure 11), confirming that current 2 is still in the slumping phase when the receding front hits the endwall. As expected, when $\tilde{t} > \tilde{T}_{LR}$, current 1 follows the theoretical prediction (1.4) for the LR regime (indicated by the solid line in figure 11). As soon as $\tilde{t} > \tilde{T}_S$, the height difference $\Delta\tilde{h}$ becomes non-zero in the upper part of the currents, say in the range $0 \leqslant \tilde{l} \leqslant \tilde{l}_D(\tilde{t})$, where $\tilde{l}_D(\tilde{t})$ denotes the downstream point reached by the reflected disturbance. As shown by the inclined line issued from the point $(\tilde{t} = \tilde{T}_S, \tilde{l} = 0)$, this disturbance propagates with a constant speed and reaches the front of current 2 at $\tilde{t} = \tilde{T}_D \approx 47$. Within the time interval $\tilde{T}_S < \tilde{t} < \tilde{T}_D$, the evolution of the front position of both currents is found to be identical, as already observed in the example of figure 10. However the novel feature in figure 11 is that, even though current 2 was not yet in the viscous regime when the endwall started to influence its dynamics, its evolution closely follows the theoretical prediction for the LR regime for $\tilde{T}_{LR} < \tilde{t} < \tilde{T}_D$. This simply confirms and extends the conclusion of figure 10 that the evolution of the downward front is not influenced by the endwall as long as it has not been reached by the reflected disturbance. In the present case, the hierarchy of times is such that $\tilde{T}_S < \tilde{T}_{LR} < \tilde{T}_D$, so that the front of the advancing current (more precisely, the downward part of the current corresponding to $\tilde{l}_D < \tilde{l} < \tilde{l}_f$) switches to the LR regime for $\tilde{t} \approx \tilde{T}_{LR}$ as if there were no endwall. Then for $\tilde{t} > \tilde{T}_D$, current 2 slows down, and the position of its front departs gradually from the LR prediction until it eventually matches the SR prediction (1.6) for $\tilde{t} \approx 170$. The situation of current 2 at $\tilde{t} = \tilde{T}_D$ is thus similar to that of any current experiencing a secondary viscous transition from the LR to the SR regime. Based on this remark,

one expects $\tilde{T}_D$ to be identical to $\tilde{T}_{LS}$. In the present example, (4.4) predicts $\tilde{T}_{LS} \approx 45.9$, which is indeed very close to the value of $\tilde{T}_D$ determined graphically from figure 11. Conversely, assuming $\tilde{T}_D = \tilde{T}_{LS}$ provides a direct means to evaluate the speed of the reflected disturbance: at time $\tilde{T}_{LS}$, (1.4) predicts $\tilde{l}_f(\tilde{T}_{LS}) = \tilde{L}_0 + \alpha Re^{1/2}\tilde{T}_{LS}^{1/2}$. Hence the disturbance travels with a speed $\tilde{c}_D = \tilde{l}_f(\tilde{T}_{LS})/(\tilde{T}_{LS} - \tilde{T}_S)$, where $\tilde{T}_S = \tilde{L}_0 Fr^{-1}$, so that $\tilde{c}_D \approx 0.40$ in the above example.

## 5. Summary and concluding remarks

To obtain some new insight on the dynamics and evolution of viscous gravity currents, we carried out extensive Navier–Stokes computations in full-depth lock-exchange configurations, for various released volumes and Reynolds numbers in the range $200 \leqslant Re \leqslant 800$. The specificity of the numerical technique employed here lies in the treatment of the equation for the volume fraction of one of the fluids (or the density field) which allows us to deal with strong gradients. Hence, in contrast with pseudo-spectral approaches, the present numerical approach makes it possible to mimic the behaviour of almost immiscible fluids, which is crucial for the comparison with experimental results and theoretical predictions in the viscous regime. We first validated our code by predicting the evolution of currents propagating in horizontal cylindrical tubes, using the theoretical and experimental results of Séon *et al.* (2007) and Takagi & Huppert (2007) in the LR and SR regimes, respectively. We then confirmed the prediction of Hinch *et al.* (2007) for the LR regime of planar currents and that of Huppert (1982) for the corresponding SR regime, whereas available experiments including ours exhibit a significant variability of the time exponent in the latter regime. We also explored the influence of three-dimensional effects on the current dynamics. In particular, we showed that the boundary layers that develop along the sidewalls result in an earlier transition to the viscous regime. We obtained a theoretical estimate of the transition time to both viscous regimes through a force balance and showed that these predictions agree well with the computed evolutions.

We finally considered the successive transitions that may happen during the 'life' of a given current. First, we derived and validated a quantitative criterion predicting which minimum (respectively maximum) released volume $\tilde{V}_{0\,c}$ is required for the LR (respectively SR) viscous regime to succeed directly the slumping phase. In cases in which the LR regime occurs, we then showed that the current later experiences a secondary viscous transition from the LR to the SR viscous regime and determined the corresponding transition time and position through a force-balance argument. Computations made it clear that in all cases, the current starts to obey the SR evolution (1.6) only at the time at which the reflected disturbance reaches the front of the advancing current, rather than at the time the receding current hits the endwall. In some cases, we observed that the LR regime sets in during the time interval separating these two events.

Keeping in mind that we focused on moderate Reynolds numbers for which the inertial regime governed by (1.3) does not occur, we may summarize our conclusions about the various 'routes' a given current may follow within a single diagram of states. This diagram is shown in figure 12. In brief, the SR regime directly succeeds the slumping phase only when the transition time $\tilde{T}_{LR}$ is larger than $\tilde{T}_{SR}$. In contrast, an intermediate LR regime exists every time $\tilde{T}_{LR} < \tilde{T}_{SR}$. In such cases, the LR regime may set in before or after the receding front hits the endwall, depending on $\tilde{T}_{LR}$ being

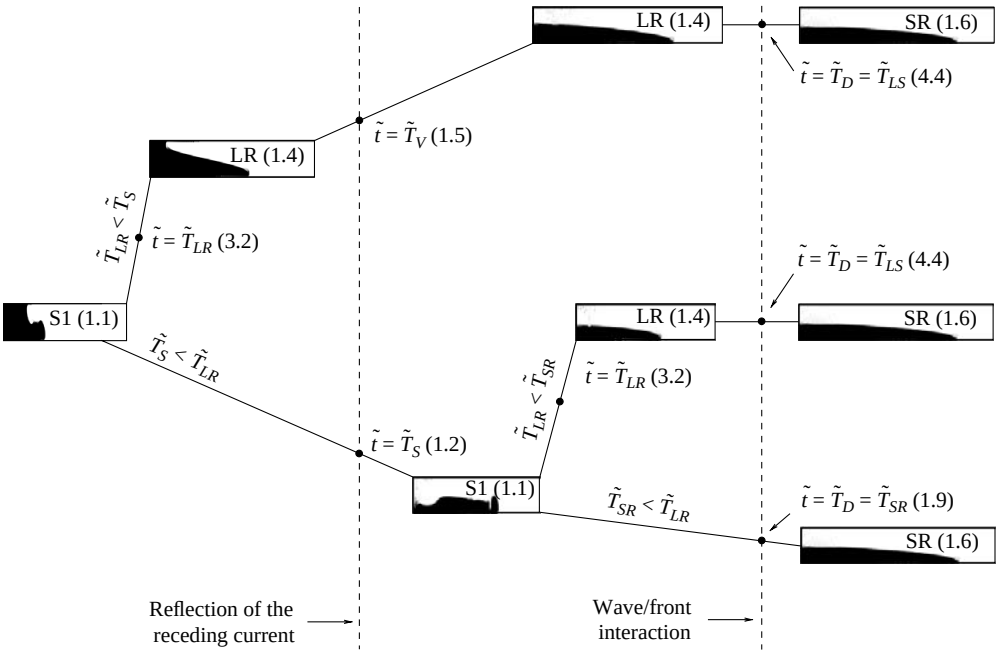


FIGURE 12. Diagram of the various possible evolutions of a given current according to the initial released volume $\tilde{L}_0$ (or $\tilde{V}_0$), Froude number $Fr$ and Reynolds number $Re$; Sl, LR and SR stand for slumping, LR and SR regimes, respectively. The numbers refer to the equation providing the expression of the corresponding transition time in terms of the above three parameters or to that providing the corresponding evolution law.

smaller or larger than $\tilde{T}_S$. Then the current experiences a second transition to the SR regime at $\tilde{t} \approx \tilde{T}_{LS}$.

We thank Annaig Pedrono for her continuous and central support in the development of the parallel version of the code used in this research. The contributions of CALMIP, CINES and IDRIS, which provided most of the CPU time, are greatly appreciated.

## REFERENCES

BENJAMIN, T. B. 1968 Gravity currents and related phenomena. *J. Fluid Mech.* **31**, 209–248.

BONOMETTI, T. & BALACHANDAR, S. 2008 Effect of Schmidt number on the structure and propagation of density currents. *Theoret. Comput. Fluid Dyn.* **22**, 341–361.

BONOMETTI, T., BALACHANDAR, S. & MAGNAUDET, J. 2008 Wall effects in non-Boussinesq density currents. *J. Fluid Mech.* **616**, 445–475.

BONOMETTI, T. & MAGNAUDET, J. 2006 Transition from spherical caps to toroidal bubbles. *Phys. Fluids* **18**, 052102.

BONOMETTI, T. & MAGNAUDET, J. 2007 A front-capturing technique for the computation of incompressible two-phase flows: validation and application to bubbly flows. *Intl J. Multiphase Flow* **33**, 109–133.

CANTERO, M. I., LEE, J. R., BALACHANDAR, S. & GARCIA, M. H. 2007 On the front velocity of density currents. *J. Fluid Mech.* **586**, 1–39.

DIDDEN, W. & MAXWORTHY, T. 1982 The viscous spreading of plane and axisymmetric gravity currents. *J. Fluid Mech.* **121**, 27–42.

Gratton, J. & Minotti, F. 1990 Self-similar viscous gravity currents: phase-plane formalism. *J. Fluid Mech.* **210**, 155–182.

Hallez, Y. & Magnaudet, J. 2008 Effects of channel geometry on buoyancy-driven mixing. *Phys. Fluids* **20**, 053306.

Härtel, C., Meiburg, E. & Necker, F. 2000 Analysis and direct numerical simulation of the flow at a gravity-current head. Part 1. Flow topology and front speed for slip and non-slip boundaries. *J. Fluid Mech.* **418**, 189–212.

Hinch, E. J., Hulin, J. P., Salin, D., Perrin, B., Séon, T. & Znaien, J. 2007 Inclined to exchange: shocking gravity currents. Http://www.damtp.com.ac.uk/user/hinch/talks/nottingham.pdf

Hoult, D. P. 1972 Oil spreading on the sea. *Annu. Rev. Fluid Mech.* **4**, 341–368.

Huppert, H. E. 1982 The propagation of two-dimensional and axisymmetric viscous gravity currents over a rigid horizontal surface. *J. Fluid Mech.* **121**, 43–58.

Huppert, H. E. 2000 Geological fluid mechanics. In *Perspectives in Fluid Dynamics* (ed. G. K. Batchelor, H. K. Moffatt & M. G. Worster), pp. 447–506. Cambridge University Press.

Huppert, H. E. & Simpson, J. E. 1980 The slumping of gravity currents. *J. Fluid Mech.* **99**, 785–799.

Linden, P. F. 1999 The fluid mechanics of natural ventilation. *Annu. Rev. Fluid Mech.* **31**, 201–238.

Marino, B. M., Thomas, L. P. & Linden, P. F. 2005 The front condition for gravity currents. *J. Fluid. Mech.* **536**, 49–78.

Necker, F., Härtel, C., Kleiser, L. & Meiburg, E. 2002 High-resolution simulations of particle-driven gravity currents. *Intl J. Multiphase Flow* **28**, 279–300.

Necker, F., Härtel, C., Kleiser, L. & Meiburg, E. 2005 Mixing and dissipation in particle-driven gravity currents. *J. Fluid Mech.* **545**, 339–372.

Rottman, J. W. & Simpson, J. E. 1983 Gravity currents produced by insantaneous releases of a heavy fluid in a rectangular channel. *J. Fluid Mech.* **135**, 95–110.

Séon, T., Znaien, J., Hinch, E. J., Perrin, B., Salin, D. & Hulin, J. P. 2007 Transient buoyancy-driven front dynamics in nearly horizontal tubes. *Phys. Fluids* **19**, 123603.

Simpson, J. E. 1982 Gravity currents in the laboratory, atmosphere, and ocean. *Annu. Rev. Fluid Mech.* **14**, 213–234.

Simpson, J. E. 1997 *Gravity Currents*. Cambridge University Press.

Takagi, D. & Huppert, H. E. 2007 The effect of confining boundaries on viscous gravity currents. *J. Fluid Mech.* **577**, 495–505.

Zalesak, S. T. 1979 Fully multidimensional flux-corrected transport algorithms for fluids. *J. Comput. Phys.* **31**, 335–362